An S-band frequency-modulated continuous-wave boundary layer profiler: Description and initial results

Türker İnce and Stephen J. Frasier

Department of Electrical and Computer Engineering, University of Massachusetts, Amherst, Massachusetts, USA

Andreas Muschinski

Cooperative Institute for Research in Environmental Sciences (CIRES), University of Colorado, and Environmental Technology Laboratory, NOAA, Boulder, Colorado, USA

Andrew L. Pazmany

Department of Electrical and Computer Engineering, University of Massachusetts, Amherst, Massachusetts, USA

Received 23 July 2002; revised 7 April 2003; accepted 19 May 2003; published 5 August 2003.

[1] Operating principles of frequency-modulated continuous-wave (FMCW) radar are reviewed, and their measurement limitations for atmospheric targets are discussed. In particular, we outline misregistration errors due to Doppler velocities and target coherence limitations on range resolution. The latter is of importance to volumetric scattering from atmospheric targets. Parallax errors and near-field operation are also considered. A high-resolution S-band FMCW radar developed at the University of Massachusetts is then described, and observations obtained by this system during the 1999 Cooperative Atmosphere-Surface Exchange Study are used to illustrate system performance. In the convective boundary layer, Rayleigh scatterers appear to dominate the observed vertical profile of mean reflectivity at S-band. *INDEX TERMS:* 0694 Electromagnetics: Instrumentation and techniques; 3307 Meteorology and Atmospheric Dynamics: Boundary layer processes; 3360 Meteorology and Atmospheric Dynamics: Remote sensing; *KEYWORDS:* boundary layer, profiler, radar

Citation: İnce, T., S. J. Frasier, A. Muschinski, and A. L. Pazmany, An S-band frequency-modulated continuous-wave boundary layer profiler: Description and initial results, *Radio Sci.*, *38*(4), 1072, doi:10.1029/2002RS002753, 2003.

1. Introduction

[2] For more than three decades, S-band, frequency-modulated, continuous-wave (FMCW) radars have been used to monitor the atmospheric boundary layer (ABL) and the lower free troposphere [*Richter*, 1969; *Eaton et al.*, 1995]. While Doppler capability can been added to FMCW radars [*Strauch et al.*, 1976], the unique strength of this technology lies in its ability to monitor the atmospheric refractive-index structure parameter, C_n^2, with unparalleled resolution in height and time.

[3] The advent of S-band FMCW radars has opened a new research field, which was reviewed by *Gossard* [1990]. Interestingly, only a handful of atmospheric FMCW radars have been built, some of which no longer exist. Those of which we are aware include: Richter's FMCW radar, the first of its kind [*Richter*, 1969]; the NOAA Wave Propagation Laboratory FMCW radar [*Chadwick et al.*, 1976; *Strauch et al.*, 1976]; the White Sands Missile Range FMCW radar [*Eaton et al.*, 1995]; the Hamburg Max Planck Institute's FMCW radar [*Hirsch*, 1996]; and the University of Massachusetts' FMCW radar, described in this paper.

[4] While S-band FMCW radars have been designed with the capability to obtain height and time resolutions of 1 m and 1 s, respectively, the degree to which these resolution limits are obtained in practice depends upon the properties of the atmospheric echo itself. Such measurement limitations can impact interpretation of radar returns. In this paper we review the theory of operation of FMCW radar including discussion of range-Doppler ambiguity, parallax typical of two-antenna radar systems, and near-field operation. We describe the radar system developed at the University of Massachusetts,

0048-6604/03/2002RS002753$11.00

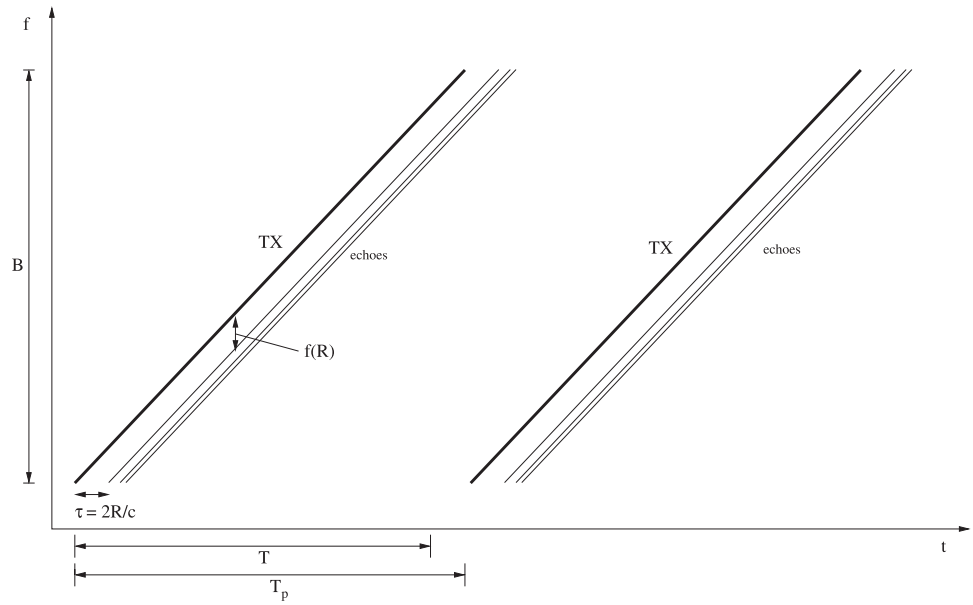

Figure 1. Frequency versus time depiction of FMCW radar transmit (TX) and receive signals delayed by $\tau = 2R/c$. Difference frequency, f(R) is given by (1).

and we illustrate system performance with data collected during recent field experiments.

2. Theory of Operation

[5] FMCW radars may be thought of as a limiting case of pulse-compression radar where the duty cycle of the transmitted waveform approaches 100%. They operate by transmitting a long, coded waveform of duration T and bandwidth B. The improvement factor they gain over pulsed radars of equivalent range resolution is given by the time-bandwidth product of the waveform BT, which is often referred to as the compression gain. In FMCW systems, this gain can be very large, exceeding 60 dB. While several types of frequency coding may be used to yield the bandwidth B, linear frequency modulation is the simplest and most commonly used method in atmospheric FMCW radars.

[6] Figure 1 shows a frequency versus time diagram of the transmitted and received echoes. The echo from an atmospheric target is essentially a delayed, attenuated, and possibly Doppler-shifted replica of the transmitted signal. By mixing the echoes with a portion of the transmitted signal, the resulting beat frequency is used to identify range. For stationary targets, the beat frequency and the range are related through the chirp rate and the travel time:

$$f(R) = \dot{f}\frac{2R}{c}, \tag{1}$$

where $\dot{f}$ is the chirp rate (B/T), R is range, and c is the speed of light. Resolving in range is done through frequency analysis of the sampled waveform - most often through a Discrete Fourier Transform.

[7] Doppler information can be retrieved on a sweep-to-sweep basis by analyzing the sequence of echoes from a particular range, as discussed by *Strauch et al.* [1976]. In this case, the sampling frequency is the reciprocal of the sweep period T_p, resulting in an unambiguous Doppler velocity interval of $u_r| \leq \frac{\lambda}{4T_p}$ where λ is the electromagnetic wavelength. A distinction is made between sweep time (T) and sweep period (T_p) to allow for duty cycle of less than 100%. Although the radar is technically not CW in this case, such operation is not uncommon, and the impact on sensitivity is inconsequential provided the duty cycle is not small compared to unity.

[8] Doppler frequency also impacts the ranging operation of FMCW radars. The sensitivity of linear FM waveforms to Doppler is treated in several radar texts [e.g., *Rihaczek*, 1985]. It can be shown (see Appendix A) that the response of the FMCW radar to a point target at range, R_0, moving at radial velocity, u_r, can be expressed as

$$y(R) = \frac{\sin[\pi(f_D T + (R - R_0))/\Delta R)]}{\pi(f_D T + (R - R_0)/\Delta R)}, \tag{2}$$

where $f_D = 2u_r/\lambda$ is the Doppler frequency, and $\Delta R = c/(2B)$ is the range resolution. The presence of both range and Doppler terms in the argument of the sinc function illustrates the effect of target motion on the

Figure 2. Photo of the University of Massachusetts S-Band FMCW radar system mounted on flatbed truck. Electronics are contained within the cab.

radar's ability to locate. Rearranging the terms in the argument in (2), the apparent range of the target is

$$R_{app} = R_0 - f_D T \Delta R, \tag{3}$$

where it is evident that misregistration by one range bin occurs when the product, $f_D T$, equals unity or when $u = \pm \frac{\lambda}{2T}$. The right-hand side of this equation corresponds to twice the Nyquist velocity interval. Thus, targets with unambiguously measured velocities are misregistered by no more than half of one range bin.

[9] Of perhaps equal concern for range resolution considerations is the coherence of the atmospheric target during the sweep interval. Implicit in the discussion of FMCW radar resolution is the assumption that the target produces a constant-frequency sinusoidal echo during the interval T. For complex moving targets or volume scattering, the coherence time (or the reciprocal of the Doppler spectral width) of the echo will limit resolution. A distribution of Doppler velocities observed over an integration time, T, will yield a distribution of apparent ranges. The resultant spreading in range is dictated by the transformation of the Doppler spectrum to the range domain using (3). The rms spread in range is given by

$$\sigma_R = \sigma_f T \Delta R, \tag{4}$$

where σ_f is the Doppler spectral width of the echo. From this relation it is apparent range resolution and sensitivity are optimized by matching the sweep time, T, to the reciprocal of the Doppler bandwidth of the echo. When this is done the range spreading is equal to the range resolution, and the entire Doppler spectrum is confined, more or less, to one range bin. No improvement in sensitivity or in resolution is achieved by increasing T beyond this value, as the resulting echo simply spreads to adjacent range bins. To maximize resolution and sensitivity, it is desirable to make both B and T as large as possible. The effective value of T is, however, constrained by the coherence time of the atmospheric echo. For example, a sampling volume with rms radial velocity of 1 m/s has a spectral width of 20 Hz at 3 GHz implying a coherence time of approximately 50 ms.

3. Instrument Description

[10] Figure 2 shows the University of Massachusetts FMCW radar system. The radar operates at S-band (2.9 GHz) with resolution and sensitivity similar to earlier FMCW radars. In its present configuration it resolves the boundary layer to 2.5 m vertical resolution. Table 1 lists the basic system characteristics of the FMCW radar. This transportable radar employs a pair of 2.4 m diameter parabolic dish antennas each with 34 dB gain, and a 250 W traveling wave tube amplifier (TWTA) transmitter. The transmitted waveform is a low-noise, 60 MHz bandwidth, linear FM sweep produced by a direct digital synthesizer (DDS). FM sweeps are repeated every 50 ms. A portion of the transmitted signal is mixed with the received signal yielding a baseband audio frequency output that is digitized using a 16-bit A/D converter. Acquired data are then processed in real time and are transferred to a host computer (PC) for display and recording.

[11] The first incarnation of this system employed a 24-bit DDS running from a 150 MHz clock. Acquired data were processed in real time using a TMS320C40 Digital Signal Processor and transferred to a personal computer. The radar has recently been upgraded with a 32-bit DDS operating from a 300 MHz clock, and data acquisition and signal processing is now performed directly on the personal computer CPU. This is made possible using a real-time variant of the Linux (Unix) operating system and eases the development of software.

[12] The radar implements an internal calibration loop by injecting into the receiver an attenuated and delayed sample of the high power amplifier output, via a surface acoustic wave (SAW) delay line. This produces a contin-

Table 1. FMCW Radar System Characteristics

	Description
Center frequency	2.94 GHz
Bandwidth	60 MHz
Transmit power	250 W
Sweep time	45 ms
Noise figure	2 dB
Range resolution	2.5 m
Height coverage	2.5 km
Antenna gain	34 dB
Antenna Beam width	3°
Polarization	single, linear

uous echo at an apparent range of 1500 m (corresponding to 10 μs delay), permitting radar system monitoring. Calibration is performed by equating the received power level through the delay line to an effective reflectivity, η_{cal} using the weather radar equation,

$$P_{cal} = \frac{P_t G A_e \eta_{cal} \Delta R \pi \Theta_1^2}{(4\pi R)^2 L_{ant} 8 \ln 2} = \frac{P_t}{L_{cal}}, \quad (5)$$

where P_{cal} and P_t are received and transmitted power, G is the antenna gain, A_e is the antenna effective aperture, ΔR is range resolution, R is effective range of the delay line echo, Θ_1 is the one-way 3 dB beam width, L_{ant} is the sum of losses in both transmit and receive antenna feedlines, and L_{cal} is the loss through the calibration path. Eliminating P_t and noting that $G\Theta_1^2 = 16 \ln 2$ for Gaussian shaped beams, we obtain an equivalent volume reflectivity of the calibration target,

$$\eta_{cal} = \frac{8\pi R^2}{A_e \Delta R} \frac{L_{ant}}{L_{cal}}, \quad (6)$$

which is subsequently used to calibrate the atmospheric echo. For Bragg scattering from refractive index fluctuations due to isotropic turbulence, η is commonly related to the refractive index structure function parameter, C_n^2 [*Tatarskii*, 1961; *Ottersten*, 1969]:

$$\eta = 0.38 C_n^2 \lambda^{-1/3}. \quad (7)$$

This relation assumes that the Bragg wavenumber, $k_B = 4\pi/\lambda$, lies within the inertial subrange. Equation (7) should be used with caution, however, as C_n^2 is defined as an ensemble average. In practice, such averaging is performed over space or time assuming ergodicity. It is the case, however, that statistically stable values for η are commonly obtained with short dwell times. For example, given an rms Doppler velocity of 1 m/s within a particular volume, there are approximately 20 independent samples available per second. Thus, (7) represents an estimate of the local refractive index structure function parameter, $\tilde{C}_n^2$. Building on *Kolmogorov* [1962] and *Oboukhov*'s [1962] similarity theory, *Peltier and Wyngaard* [1995] explored the variability of $\tilde{C}_n^2$ obtained using the large-eddy simulation (LES) technique. *Muschinski et al.* [1999] used a single LES-generated realization of the turbulent refractive-index and velocity fields to synthesize radar wind profiler signals based on first principles [*Tatarskii*, 1961]. They used the synthesized signals to study effects of $\tilde{C}_n^2$ inhomogeneity on estimated Doppler velocities. *Pollard et al.* [2000] compared $\tilde{C}_n^2$ statistics extracted from LES-generated fields with statistics of local radar reflectivity observed with a volume-imaging radar wind profiler.

[13] It is common for atmospheric FMCW radars to employ separate antennas for transmission and reception.

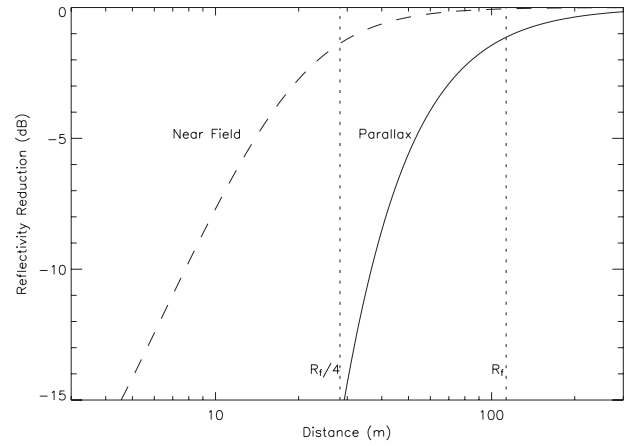

Figure 3. Reflectivity reduction due to parallax (solid line) and near-field (dashed line) effects for the parameters of the FMCW radar. Dotted lines indicate the far-field distance, R_f, and one fourth this distance.

This is done out of necessity because of the need for high isolation between the transmitter and receiver. Standard duplexers such as ferrite circulators are usually limited to isolations of 25–30 dB, but it is not unusual for FMCW radars to require transmitter/receiver isolations of the order 100 dB. Because the FMCW radar employs two spatially separated antennas, a correction of the received power is necessary at near ranges to account for the reduced beam overlap. For Gaussian shaped beams aligned with their center axes parallel, the antenna parallax function, or fractional beam overlap, is (see Appendix B)

$$c_p(R) = \exp\left(-2 \ln 2 \frac{d^2}{(\Theta_1 R)^2}\right) \quad (8)$$

where d is the separation distance between transmit and receive antennas, and Θ_1 is the one-way half-power beam width. Parallax results in an apparent reflectivity reduction. Figure 3 shows this function plotted versus height for separation $d = 2.75$ m and beam width $\Theta_1 = 3°$, the parameters of this system. The parallax-induced "decorrelation height" (the height at which $c_p = e^{-1}$) occurs at 62 m.

[14] It is perhaps of some concern that the decorrelation height occurs within the radiating near field of the antennas such that assumption of a far-field Gaussian beam pattern is suspect. In their analysis, *Eaton et al.* [1995] show a similar curve computed numerically, but were careful to indicate that it does not apply within the near field. Instead they used an ad hoc empirical correction. We believe (8) is reasonably applicable to ranges as close as one fourth the far-field distance, $R_f/4 = D^2/(2\lambda)$ which is approximately 30 m for this system. Noting that the far-field criterion, $R_f = 2D^2/\lambda$, is based on a conser-

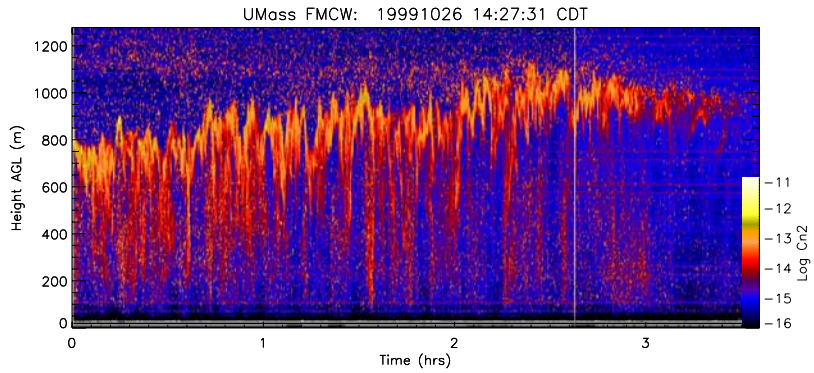

Figure 4. Afternoon convective boundary layer observed on 26 October 1999 beginning at 14:27 CDT.

vative specification of maximum phase error, significant effects on the shape of the main lobe are not evident until $R \approx R_f/4$. *Hansen* [1985] show that the directivity of a circular aperture is reduced by only 20% at this distance resulting in a 1.9 dB reduction in two-way gain. *Sekelsky* [2002] has obtained a universal near-field reflectivity correction that indicates a 1 dB reduction in reflectivity at $R_f/4$ (reflectivity is a beam-integrated quantity, while boresight gain is not). At closer ranges, the gain reduction becomes much more significant. Associated with the reduced gain is a broadening of the beam and filling of sidelobes. Beam broadening, the first order effect on parallax, is small for $R > R_f/4$, but again, increases rapidly for $R < R_f/4$. Thus, at closer ranges, the beam shape is no longer approximately Gaussian and is strongly dependent upon the particular antenna design. To compare the relative importances of near field gain reduction and parallax, *Sekelsky*'s [2002] near-field reflectivity correction is also plotted in Figure 3. For the parameters of the University of Massachusetts system, it is clear that parallax has the primary influence at close ranges.

4. Sample Observations

[15] The University of Massachusetts S-band FMCW radar was first operated during the 1999 Cooperative Atmosphere-Surface Exchange Study (CASES-99) experiment, during which a wide range of boundary layer and micrometeorological instrumentation was deployed near Leon, Kansas [*Poulos et al.*, 2002]. During the experiment the radar was located approximately 400 m northeast of a 55 m instrumented tower and 300 m south of a radiosonde launch site. The radar was oriented vertically and configured with a sweep time of 45 ms and a sweep period of 53 ms (85% duty cycle). Collected data were processed and transferred to disk during the 8 ms gap. Data processing consisted of DC bias removal followed by spectral analysis via FFT to obtain height profiles. A Hanning window was applied prior to the FFT to suppress range sidelobes. Data were then treated in 100 profile blocks (5.3 s) where for each range bin, received power was calculated from the variance of the 100 sample record. Echoes from fixed targets (delay line, ground clutter) were obtained from the squared mean voltage over the dwell time, but were subtracted from the signal prior to calculating variance. Finally, an estimate of the receiver thermal noise obtained from distant range bins was subtracted from every pixel.

[16] Figure 4 shows an afternoon convective boundary layer observed on 26 October beginning at 14:30 local time (CDT, or 19:30 UTC). Meteorological conditions for the afternoon were clear skies with a temperature of 25 C, relative humidity of 22%, and southerly wind speed of 4–5.5 m/s. The radar echo is expressed in terms of the logarithm of C_n^2 obtained using (7). It should be noted that this representation is only meaningful for the clear-air component of the backscatter described by the Bragg scattering mechanism. Given the vertical orientation of the antennas, only vertical velocities contribute to misregistration, which is estimated to be about one range bin at most.

[17] In addition to distributed Bragg scatter from clear air, Figure 4 shows strong "dot echoes." Although these are commonly interpreted as echoes from Rayleigh scatterers such as insects [*Gossard*, 1990; *Eaton et al.*, 1995], similar echo signatures may be expected for Bragg scatter from highly intermittent, high Reynolds-number refractive-index turbulence, where C_n^2 tends to be lognormally distributed in time [*Frehlich*, 1992]. It is beyond the scope of this paper to consider possible clear-air contributions to observed dot echoes. Instead we adopt the traditional, though perhaps oversimplifying, view that they are entirely due to Rayleigh scatterers.

[18] During the initial phase of the record in Figure 4, significant Rayleigh backscatter is observed both above

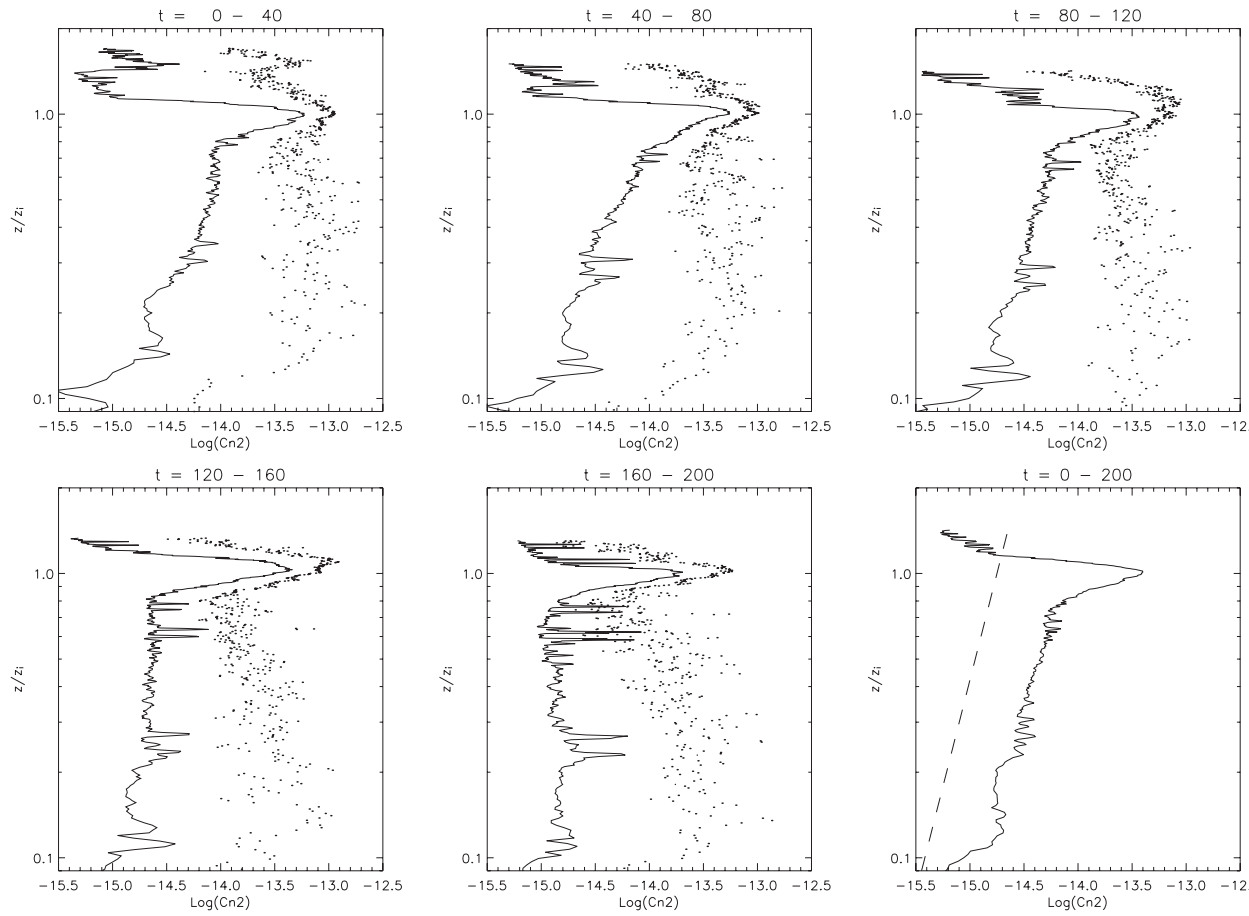

Figure 5. Vertical profiles of estimated C_n^2 (solid lines) obtained from median reflectivity over five consecutive 40-min periods and over entire period (bottom right). Dotted profiles show the mean reflectivity including both Bragg and Rayleigh echo.

and below the capping inversion which peaks near 1 km altitude at about 17:00 local time. After this time, both the Rayleigh scatter and the distributed Bragg scatter below the inversion decrease significantly, the temperature begins to drop, and the strong echo at the top of the boundary layer disappears.

[19] Figure 5 shows vertical profiles of radar reflectivity for consecutive 40-min segments. Given the mean horizontal winds, the vertical profiles are roughly equivalent to a streamwise spatial average over approximately 10 km. The vertical axis of each profile is scaled by the boundary layer depth, z_i, obtained (by eye) from the maximum of the reflectivity. Solid lines indicate estimated clear-air component of the vertical profile obtained from the median value of the reflectivity observed over the 40-min interval. The median was chosen to suppress the influence of Rayleigh echoes. The dotted profiles show the mean reflectivity over the same intervals including both Bragg and Rayleigh echo. In this case, the Rayleigh component appears to dominate the observed profiles of mean reflectivity.

[20] In the mixed layer, C_n^2 is expected to follow a $z^{-4/3}$ power law, where z is height above ground level [*Wyngaard and LeMone*, 1980; *Gossard and Strauch*, 1983]. We find that this profile is not observed here even after attempts to remove the resolvable Rayleigh echo. Averaged over the time period, we find the profile follows a $z^{+2/3}$ profile, a discrepancy of z^2. Interestingly, such behavior has also been observed with the U.S. Army FMCW Radar [*Eaton et al.*, 1995] during its deployment in the Profiler-HELIPOD Intercomparison Experiment in November 1997 along the central Pacific coast. The observed discrepancy may be due to a combination of factors including an inability to remove all (or enough of) the Rayleigh echo, and the influence of significant downward mixing from the entrainment region as suggested by ''top-down, bottom-up'' diffusion models [*Fairall*, 1987].

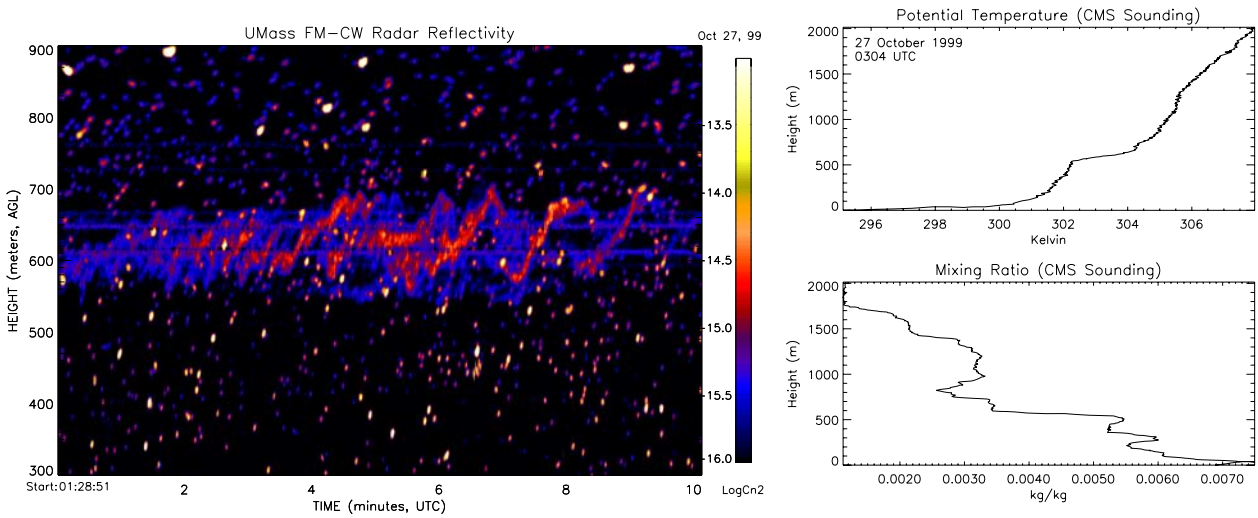

Figure 6. (left) Kelvin-Helmholtz billows in the residual layer observed at 0130 UTC on October 27. (right) Radiosonde profiles of potential temperature and water vapor mixing ratio at 0304 UTC.

[21] Figure 6 shows a Kelvin-Helmholtz billow event observed later in the evening at approximately 600 m height. Although a coincident sounding was not available, the nearest sounding at 0300 UTC shows a stable profile with strong gradients in the temperature and water vapor mixing ratio profiles at approximately 500 m height. The apparent width of the billow "filaments" is a few range bins, or about 10 m. The maximum crest-to-trough amplitude is about 100 m.

[22] Early in the morning of 27 October a low-level jet formed with maximum winds of over 16 m/s at approximately 300 m height (Figure 7). The FMCW radar shows turbulence in the nocturnal boundary layer, which extended to heights of about 150 m where the sounding shows evidence of strong shear. A layer of insects is observed at heights of the wind speed maximum.

5. Summary

[23] The University of Massachusetts has developed an S-band FMCW atmospheric radar, the latest in a series of such instruments developed by various groups since the

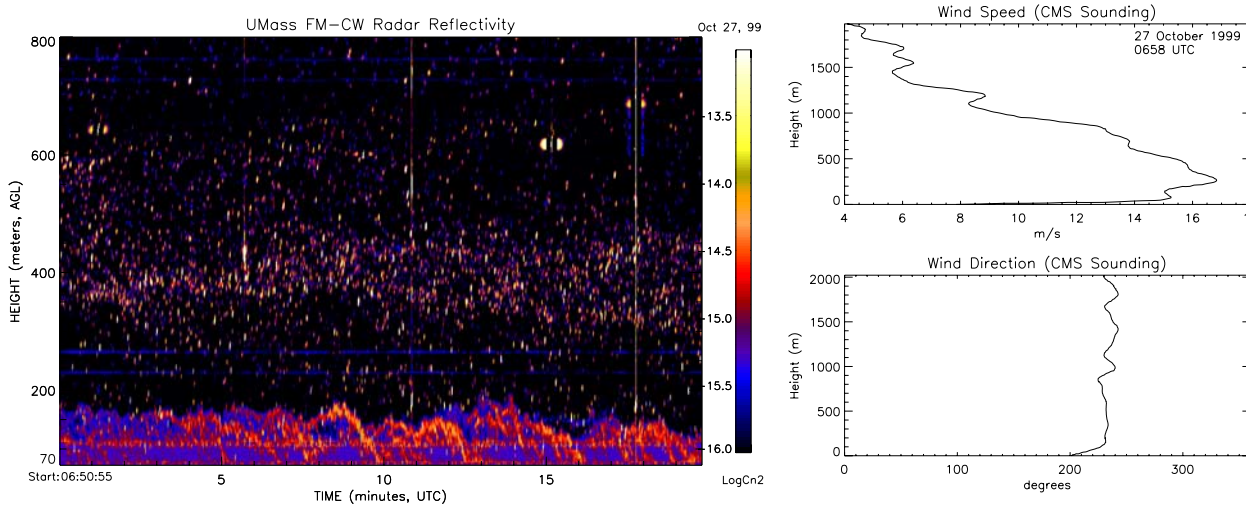

Figure 7. (left) Nocturnal boundary layer turbulence below and insects within a low-level jet observed at 0650 UTC. (right) Radiosonde profiles of wind speed and wind direction at 0658 UTC.

late 1960s. Operating principles and measurement limitations were reviewed. For the parameters of this system, targets with radial velocities within ±0.5 m/s are registered properly, and distributed scatter with rms velocity $\leq$1 m/s is not significantly degraded. Parallax has the dominant effect on reflectivity within the near field of the antennas. Sample observations from the CASES-99 experiment show the sensitivity of the radar to both Bragg and Rayleigh scatterers.

Appendix A: FMCW Signal Analysis

[24] Consider a transmitted linear-FM signal of the form

$$s(t) = \exp\left(j\omega t + j\frac{1}{2}at^2\right) \quad -T/2 < t < T/2 \tag{A1}$$

where ω is the radian frequency and a is the chirp rate in rad/s^2. The radar echo from a target located a distance, R, from the transmitter is an attenuated copy of $s(t)$ delayed by $\tau = 2R/c$, where c is the speed of light. The echo is demodulated by mixing it with a copy of the transmitted signal and low-pass filtering the result, or mathematically

$$r(t) = \langle s(t-\tau)s^*(t)\rangle \tag{A2}$$

where * indicates the complex conjugate. Upon demodulation

$$r(t) = \exp\left[-j\left(2kR + \frac{2R}{c}at - a\frac{4R^2}{c^2}\right)\right], \tag{A3}$$

and by expressing the range to the target as $R = R_0 + ut$, we can observe the response to motion at radial velocity, u. In doing so, the last term in the exponential in (A3) may be safely ignored for nonrelativistic velocities. Insertion in (A3) yields

$$r(t) = \exp\left[-j\left(2kut + \frac{2R_0}{c}at + \frac{2u}{c}at^2\right)\right], \tag{A4}$$

where constant phase terms have been omitted. The instantaneous frequency of $r(t)$ is obtained from the time derivative of the phase,

$$f_r(t) = -\left(\frac{2u}{\lambda} + \frac{2R_0}{c}\dot{f} + \frac{4u}{c}\dot{f}t\right), \tag{A5}$$

where λ is the electromagnetic wavelength and where $\dot{f} = a/2\pi$ is the chirp rate in Hz/s. Here, the first term represents the Doppler frequency shift, f_D, due to radial motion, and the second term represents the shift due to the nominal range of the target. It is this second term that is exploited primarily by the FMCW radar. The final term represents a defocusing due to the dialation or compression of the reflected signal's bandwidth due to the dependence of Doppler frequency to carrier frequency.

[25] The relative impact of the last term is more clearly seen by considering the change in frequency of a detected echo over the sweep interval T. Evaluating (A5) at the limits $t = \pm T/2$ yields

$$\Delta f_r = f_r(T/2) - f_r(-T/2) = \frac{2u}{c}\dot{f}T. \tag{A6}$$

Thus, not only is the echo offset by the mean Doppler frequency, but the slope of the sweep is also changed slightly. The bandwidth of the echo is given by [*Rihaczek*, 1985]

$$B' = B\left(1 - \frac{2u}{c}\right). \tag{A7}$$

This becomes a measureable, though negligible, effect for velocities >100 m/s. For lower atmospheric velocities, this may be safely ignored.

[26] Signal processing of the echo usually involves matched filtering or, equivalently, correlating the echo with a conjugate phase signal,

$$m(t) = \exp\left(j\frac{2R}{c}at\right) \tag{A8}$$

which describes the echo of a stationary target at range R. The output of the matched filter is then

$$y(R) = \frac{1}{T}\int_{-T/2}^{T/2} r(t)m(t)dt = \frac{\sin[\pi(f_D T + (R-R_0)/\Delta R)]}{\pi(f_D T + (R-R_0)/\Delta R)} \tag{A9}$$

where f_D is the Doppler frequency and $\Delta R = c/(2B)$ is the expected range resolution for a transmitted bandwidth $B = \dot{f}T$. Matched filtering is most commonly implemented for all ranges simultaneously through spectral analysis via an FFT algorithm. Some form of windowing is usually used to reduce range sidelobes to an acceptable level.

Appendix B: Parallax Correction

[27] Assuming a simple Gaussian model as suggested, for example, by *Doviak and Zrnic* [1984], the one-way power weighting function of an antenna may be described by

$$G(x,y) = \exp\left(-\frac{x^2+y^2}{2\sigma_t^2}\right), \tag{B1}$$

where the antenna center is located at $x = 0$ and $y = 0$, and where σ_t is a measure of the transverse diameter of the scattering volume centered at range, R:

$$\sigma_t^2 = \sigma_\Theta^2 R^2 = \frac{\Theta_1^2}{8 \ln 2} R^2 \tag{B2}$$

where Θ_1 is the one-way, half-power beam width. The parallax correction factor, c_P, for a vertically pointing, bistatic configuration with antenna separation d is obtained by assuming that the transmitting antenna is located at $x = -d/2$ and $y = 0$, and the receiving antenna is located at $x = +d/2$ and $y = 0$. Then, c_P is expressed as the ratio of the two-way bistatic antenna pattern to the two-way monostatic pattern centered at $x = 0$, $y = 0$:

$$\begin{aligned} c_P &= \frac{\int G(x - d/2, y) G(x + d/2, y) dxdy}{\int G^2(x, y) dxdy} \\ &= \frac{\int \exp\left(- \frac{(x - d/2)^2 + y^2 + (x + d/2)^2 + y^2}{2\sigma_t^2} \right) dxdy}{\int \exp\left(- \frac{x^2 + y^2}{\sigma_t^2} \right) dxdy} \\ &= \exp\left(- \frac{d^2}{4\sigma_t^2} \right) \frac{\int \exp\left(- \frac{x^2 + y^2}{\sigma_t^2} \right) dxdy}{\int \exp\left(- \frac{x^2 + y^2}{\sigma_t^2} \right) dxdy} \\ &= \exp\left(-2 \ln 2 \frac{d^2}{\Theta_1^2 R^2} \right) = \exp\left(- \frac{R_c^2}{R^2} \right), \end{aligned} \tag{B3}$$

where

$$R_c = \sqrt{2 \ln 2} \frac{d}{\Theta_1} \tag{B4}$$

is the range below which the parallax error of the backscattered power becomes larger than $e = 2.71 = 4.3$ dB. In the case of the University of Massachusetts FMCW radar, we have $R_c = 62$ m.

[28] **Acknowledgments.** The authors thank J. K. Lundquist for providing the radiosonde observations and Ken Moran and two anonymous reviewers for their helpful comments on the manuscript. This work was supported by grants from the U.S. Army Research Office (Atmospheric Sciences: DAAG-55-98-1-0480), the Defense University Research Instrumentation Program, and the U.S. Department of Energy under the auspices of the Environmental Meteorology Program of the Office of Biological and Environmental Research.

References

Chadwick, R. B., K. P. Moran, R. G. Strauch, G. E. Morrison, and W. C. Campbell, Microwave radar wind measurements in the clear air, *Radio Sci.*, *11*, 795–802, 1976.

Doviak, R. J., and D. S. Zrnic, Reflection and scatter formula for anisotropically turbulent air, *Radio Sci.*, *19*, 325–336, 1984.

Eaton, F. D., S. A. McLaughlin, and J. R. Hines, A new frequency-modulated continuous wave radar for studying planetary boundary layer morphology, *Radio Sci.*, *30*, 75–88, 1995.

Fairall, C. W., A top-down and bottom-up diffusion model of C_T^2 and C_Q^2 in the entraining convective boundary layer, *J. Atmos. Sci.*, *44*, 1009–1017, 1987.

Frehlich, R., Laser scintillation measurements of the temperature spectrum in the atmospheric surface layer, *J. Atmos. Sci.*, *49*, 1494–1509, 1992.

Gossard, E. E., Radar research on the atmospheric boundary layer, in *Radar in Meteorology*, edited by D. Atlas, pp. 477–527, Am. Meteorol. Soc., Boston, 1990.

Gossard, E. E., and R. G. Strauch, *Radar Applications in Cloud and Clear Air*, 191 pp., Elsevier Sci., New York, 1983.

Hansen, R. C., Aperture theory, in *Microwave Scanning Antennas*, vol. 1, edited by R. C. Hansen, Penninsula, Los Altos, Calif., 1985.

Hirsch, L., Spaced-antenna-drift measurements of the horizontal wind speed using a FMCW-radar-RASS, *Contrib. Atmos. Phys.*, *69*, 113–117, 1996.

Kolmogorov, A. N., A refinement of previous hypotheses concerning the local structure of turbulence in a viscous incompressible fluid at high reynolds number, *J. Fluid Mech.*, *13*, 82–85, 1962.

Muschinski, A., P. P. Sullivan, D. B. Wuertz, R. J. Hill, S. A. Cohn, D. H. Lenschow, and R. J. Doviak, First synthesis of wind-profiler signals on the basis of large-eddy simulation, *Radio Sci.*, *34*, 1437–1459, 1999.

Oboukhov, A. M., Some specific features of atmospheric turbulence, *J. Fluid Mech.*, *13*, 77–81, 1962.

Ottersten, H., Atmospheric structure and radar backscattering in clear air, *Radio Sci.*, *4*, 1179–1193, 1969.

Peltier, L. J., and J. C. Wyngaard, Structure-function parameters in the convective boundary layer from large eddy simulation, *J. Atmos. Sci.*, *52*, 3641–3660, 1995.

Pollard, B. D., S. Khanna, S. J. Frasier, J. C. Wyngaard, D. W. Thomson, and R. E. McIntosh, Local structure of the convective boundary layer from a volume-imaging radar, *J. Atmos. Sci.*, *57*, 2281–2296, 2000.

Poulos, G. S., et al., Cases-99: A comprehensive investigation of the stable nocturnal boundary layer, *Bull. Am. Meteorol. Soc.*, *83*, 555–581, 2002.

Richter, J., High-resolution tropospheric radar sounding, *Radio Sci.*, *4*, 1261–1268, 1969.

Rihaczek, A., *Principles of High Resolution Radar*, Penninsula, Los Altos, Calif., 1985.

Sekelsky, S. M., Near-field reflectivity and antenna boresight gain corrections for millimeter wave atmospheric radars, *J. Atmos. Oceanic Technol.*, *19*, 468–477, 2002.

Strauch, R. G., W. C. Campbell, R. B. Chadwick, and K. P. Moran, Microwave FM-CW Doppler radar for boundary layer probing, *Geophys. Res. Lett.*, *3*, 193–196, 1976.

Tatarskii, V. I., *Wave Propagation in a Turbulent Medium*, McGraw-Hill, New York, 1961.

Wyngaard, J. C., and M. A. LeMone, Behavior of the refractive index structure parameter in the entraining convective boundary layer, *J. Atmos. Sci.*, *37*, 1573–1584, 1980.

S. J. Frasier, T. İnce, and A. L. Pazmany, Department of Electrical and Computer Engineering, University of Massachusetts, Amherst, MA 01003, USA. (frasier@ecs.umass.edu)

A. Muschinski, Environmental Technology Laboratory, NOAA, 325 Broadway, Boulder, CO 80305-3328, USA.